



HAL
open science

Low temperature strengthening and dislocation substructure of (112) [111] anti-twinning slip system in α -iron

G. Coulon, B. Escaig

► **To cite this version:**

G. Coulon, B. Escaig. Low temperature strengthening and dislocation substructure of (112) [111] anti-twinning slip system in α -iron. *Journal de Physique*, 1976, 37 (11), pp.1363-1372. 10.1051/jphys:0197600370110136300 . jpa-00208534

HAL Id: jpa-00208534

<https://hal.science/jpa-00208534>

Submitted on 4 Feb 2008

HAL is a multi-disciplinary open access archive for the deposit and dissemination of scientific research documents, whether they are published or not. The documents may come from teaching and research institutions in France or abroad, or from public or private research centers.

L'archive ouverte pluridisciplinaire **HAL**, est destinée au dépôt et à la diffusion de documents scientifiques de niveau recherche, publiés ou non, émanant des établissements d'enseignement et de recherche français ou étrangers, des laboratoires publics ou privés.

Classification
 Physics Abstracts
 9.126

LOW TEMPERATURE STRENGTHENING AND DISLOCATION SUBSTRUCTURE OF $(\bar{1}\bar{1}2)$ $[\bar{1}\bar{1}\bar{1}]$ ANTI-TWINNING SLIP SYSTEM IN α -IRON

G. COULON and B. ESCAIG

Laboratoire de Structures et Propriétés de l'Etat Solide (*)
 Université des Sciences et Techniques de Lille
 BP 36, 59650 Villeneuve-d'Ascq, France

(Reçu le 20 avril 1976, révisé le 8 juin 1976, accepté le 24 juin 1976)

Résumé. — La consolidation du fer α monocristallin a été étudiée sur le système $(\bar{1}\bar{1}2)$ $[\bar{1}\bar{1}\bar{1}]$ entre 123 K et 296 K jusqu'à 40 % de déformation. Les paramètres d'activation thermique ont été mesurés tout le long de la courbe de déformation par relaxation de la contrainte appliquée et par des essais différentiels en fluage ; parallèlement, on a examiné la sous-structure de dislocations par topographie X de Berg-Barrett. Tout comme dans une étude précédente faite sur le système $(\bar{1}01)$ $[111]$, et en dépit des conditions différentes d'orientation, le frottement de réseau joue encore un rôle prépondérant en dessous de 200 K. Au contraire, à haute température, le durcissement est différent ; il présente un stade I associé à une sous-structure de dislocations homogène et un stade II correspondant à une sous-structure hétérogène.

Abstract. — α -iron single crystals have been investigated in the so-called $(\bar{1}\bar{1}2)$ $[\bar{1}\bar{1}\bar{1}]$ anti-twinning slip system between 123 and 296 K, up to 40 % deformation. Stress relaxation and creep tests have been used to measure activation parameters continuously during tensile straining. Berg-Barrett X-Ray reflection topography was used to examine the overall dislocation substructure. In agreement with a previous study on the $(\bar{1}01)$ $[111]$ slip system, we confirm the strong influence of lattice friction below about 200 K, despite the very different orientation conditions. In contrast, the strengthening behaviour found at higher temperatures is different, and there is a two stage stress-strain curve : stage I is clearly associated with homogeneous dislocation substructure, while in stage II it is definitely heterogeneous.

1. Introduction. — The low temperature work-hardening of pure b.c.c. metals, and the kind of dislocation cellular substructure which is developed under conditions of a high intrinsic lattice friction, is still an open field. In a previous work [1], hereafter called Part I, we studied the low temperature plastic behaviour of α -iron single crystals deformed on the $(\bar{1}01)$ $[111]$ slip system up to 0.2 tensile strain. We found the mechanism controlling work-hardening is quite different on both sides of a transition temperature : above 200 K, the thermally decreasing lattice friction allows primary and conjugate slip systems to interact, so dislocation sheets along the two slip planes are left throughout the whole crystal and give rise to some constant work hardening rate. On the contrary below 200 K, the lattice friction becomes high enough to prevent any dislocation rearrangement and controls alone the whole plasticity : the stress-strain curves show an almost zero work-hardening rate.

The peculiar tensile axis orientation investigated did not allow us, however, to observe above 200 K several hardening stages, in contrast with some other experimental studies of b.c.c. metals [2 to 8]. Therefore, we felt it necessary to study on another slip system what influence the orientation exerts upon the substructure evolution. Also, amounts of strain had to be limited to only 0.2 in Part I in order to avoid profuse twinning at 150 K and below.

This paper reports on the low temperature plastic behaviour of the so-called $(\bar{1}\bar{1}2)$ $[\bar{1}\bar{1}\bar{1}]$ anti-twinning slip system. As compared with Part I, the present tensile orientation (1) has a much less competitive conjugate slip system and (2) gives a zero Schmid factor on the cross-slip plane common to the primary and conjugate system, two features which are expected to be significant for producing a quite different slip polygonisation. Tensile strains up to 0.4 have been produced by pure slip between room temperature down to 123 K, and standard techniques (creep tests, constant strain-rate tensile tests, stress relaxations)

(*) Laboratoire associé au C.N.R.S., n° 234.

have been extensively used and correlated to direct observations of the dislocation substructure at the sample scale, through Berg-Barrett X-ray topographs all through the investigated range.

In agreement with the general picture obtained in Part I, we still confirm the strong influence of Peierls — or lattice — friction below about 200 K, despite the very different orientation conditions. In contrast, the strengthening behaviour found at higher temperatures is different, and shows a two-stage stress-strain curve; stage I is clearly associated with homogeneous dislocation substructure, while in stage II it is definitely heterogeneous. The nature of the tangles, as well as their effects on the work-hardening rate are almost opposite on the two sides of the temperature 225 K.

In section 2, the different experimental procedures are described; section 3 is devoted to the geometry of the present orientation, then results are given in section 4 and we come to a conclusion in section 5.

2. Experimental procedures. — **2.1 PLASTIC DEFORMATION.** — Two large as-grown single crystals ($300 \times 35 \times 1.2 \text{ mm}^3$), A and B in the following, were supplied by IRSID. They contained about 20 p.p.m. (wt) nitrogen and 100 p.p.m. (wt) carbon.

Tensile samples were mechanically cut from these using a gauge, to dimensions $14 \text{ mm} \times 3 \text{ mm}^2$, with a tensile axis near to $[\bar{3}31]$. The Schmid factor on the $(112) [\bar{1}\bar{1}\bar{1}]$ slip system is about 0.5.

Specimens were then chemically polished and purified by annealing in wet hydrogen, first at 500 C for 16 hours, then at 720 C for 24 hours, and finally in dry hydrogen at 720 C for 9 hours. Carbon analyses of samples A and B were performed by burning in oxygen atmosphere. They gave carbon contents reduced respectively to 90 p.p.m. (wt) in samples A and to 16 p.p.m. (wt) in samples B. This difference for apparently similar treatments was not explained.

Tensile tests were conducted in an Instron machine imposing a constant shear strain rate

$$\dot{\gamma} = 2.5 \times 10^{-5} \text{ s}^{-1}.$$

Creep tests were performed in tension using a dead weight machine built in our laboratory [9, 10]. Controlled temperature baths (ethyl-alcohol or isopentane) were used at 295, 250, 225, 200, 150 and 123 K.

The resolved shear stress τ and strain γ are calculated from the appropriate single-slip formula [11].

Activation volumes (V/b^3) are obtained at 295, 250, 225 and 200 K by stress relaxation technique throughout the constant strain rate tests, and by stress jumps during the (logarithmic) creep tests [12].

2.2 THE BERG-BARRETT METHOD. — The Berg-Barrett X-ray technique and the origin of the different observed contrasts have been described previously in many papers [1, 13, 14, 15]. However, in order to facilitate the understanding of X-ray topographs we recall, briefly, that linear defects in a crystal give rise to two kinds of contrasts :

— *Extinction contrast* due to primary extinction phenomenon : on topographs contrast lines appear as *black lines* on a grey background.

— *Misorientation contrast* due to local rotations of the lattice. This contrast allows us to estimate for a given dislocation wall formed during straining, both its tilt-twist character and the lattice misorientation it produces. Let Ω be the rotation axis of the wall; if it has a component about the normal to the incident plane, a black and white contrast — the so-called *orientation contrast* — features the wall on topographs and is a direct measure of the net lattice misorientation across it, i.e. of the number of + or — dislocations in excess. If on the other hand, Ω has a non-vanishing component about the intersection between the reflecting and the incident planes, it causes the X-ray beam to be deviated perpendicularly to the incident plane; this shift gives rise to the *displacement contrast* made visible by the very characteristic offset it produces on some other contrast line at its crossing with the cell wall. In principle the tilt-twist nature of the wall could be deduced from the type of offset (see Fig. 1a, 1b) but most generally the wall is a kink wall, i.e. produces an almost balanced + and — lattice rotation; in this case, the wall induces merely a symmetrical cusp-shaped deformation of the contrast line it crosses, which is practically not very different in the two cases (Fig. 1c, 1d). All that can be extracted from such cusps, then, is the number of those dislocations in the wall which equilibrate their sign, which determines the cusp height for a given crystal-film spacing.

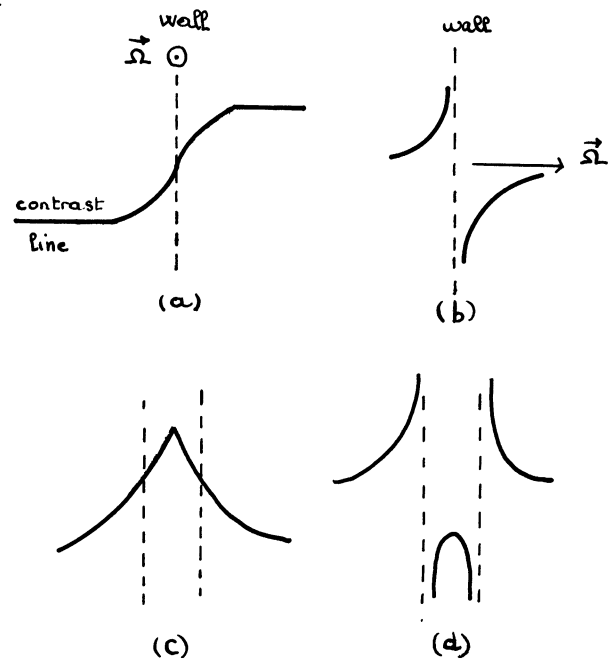


FIG. 1. — Displacement contrast : a) produced by a tilt wall containing dislocations of a given sign ; b) produced by a twist wall containing dislocations of a given sign ; c) produced by a tilt wall containing dislocations of opposite signs ; d) produced by a twist wall containing dislocations of opposite signs.

In short, the scale of the Berg-Barrett observations, somewhat similar to that of etch-pits, give a unique overall view of the work-hardening substructures; some characteristic features are thus made visible, which could not have been noticed on a much smaller scale, e.g. with electron microscopy.

In the present case, topographs are obtained from the sample after acid polishing on two different surfaces: the lamella plane (near to (001) plane) and the edge plane (near to $(\bar{1}10)$ plane). The reflections used are $\mathbf{g} = (001)$ for the (001) face and $\mathbf{g} = (\bar{1}00)$, (010), or (110) for the $(\bar{1}10)$ face.

For the sake of clarity, note that the edge plane contains the primary and conjugate slip directions, and that primary and conjugate slip planes have the same trace $[\bar{1}\bar{1}0]$ on the lamella plane.

3. Special geometry of this orientation. — The purpose of this section is to display the main geometrical features of our orientation and their consequences on the deformation.

3.1 CONJUGATE SLIP SYSTEM. — The conjugate slip system is $(\bar{1}\bar{1}\bar{2})[\bar{1}\bar{1}1]$; it has a relatively small Schmid factor ($\varphi = 0.38$) so it should be much less active than in Part I. Therefore conjugate slip is expected to occur only at a rather high strain.

3.2 TRANSFER CROSS-SLIP PLANE. — In part I, we suggested that screw cross-slipping in an *essential step* for dislocation rearrangements, sheet formations, and finally partial release of long range stress fields in the course of deformation. This is because the cross-slip plane acts as the needed *transfer plane* between the attractive dislocations formed in the crystal: either it would be between two opposite primary screws, or between a primary and an attractive conjugate dislocation. In this last case, both dislocations develop mainly as screws, due to the lattice friction; therefore they can only *polygonise* and feed the crude kind of walls which are observed if they run parallel along a length long enough instead of forming just a junction. Thus, at least one of them has to cross-slip first on that cross-slip plane which contains both primary and conjugate Burgers vectors, which we call the *transfer plane*.

Note also that this transfer plane is the only one for which both the primary and conjugate screws produced during straining make no forest obstacles. It is therefore expected to play a key role in the work-hardening behaviour of b.c.c. metals, as it does in some experiments where it has been named the *anomalous slip plane* [17].

In the present case, the transfer cross-slip plane is the edge plane of the specimen, $(\bar{1}\bar{1}0)$, and has a zero Schmid factor while it was 0.25 in part I. Therefore cross-slip transfers should be more difficult, and the resulting dislocation substructure is expected to be different, as is observed.

3.3 POSSIBLE SLIP POLYGONISATION. — In order to make easier the interpretation of the topographs, a useful guess of the nature of expected tangles can be drawn from inspection of what a *perfect* slip polygonisation should look like, even though we know that it is actually built up more crudely. If we suppose that dislocations are not allowed to climb, and if we consider only the interaction between primary and conjugate dislocations, then a straight-forward application of the Frank formula [16] yields all the possible subgrain boundaries without long range stress fields which can be formed. These are given in table I.

TABLE I

Possible subgrain boundaries without long-range stress fields in iron. Ω is the subgrain boundary rotation axis and \mathbf{v} its normal.

$$\text{Two families } \mathbf{b}_1 = \frac{1}{2}[\bar{1}\bar{1}\bar{1}] \text{ and } \mathbf{b}_2 = \frac{1}{2}[\bar{1}\bar{1}1].$$

(1) *Parallel dislocations*

a) different slip planes: $(\bar{1}\bar{1}\bar{2})$ and $(\bar{1}\bar{1}\bar{2})$

$$\left\{ \begin{array}{l} \Omega = [\bar{1}\bar{1}0] \\ \mathbf{v} \perp [\bar{1}\bar{1}0] \end{array} \right.$$

primary and conjugate dislocations are edge dislocations parallel to $[\bar{1}\bar{1}0]$;

b) identical slip plane: $(\bar{1}\bar{1}0)$

$$\left\{ \begin{array}{l} \Omega \text{ non fixed} \\ \mathbf{v} \perp [\bar{1}\bar{1}0] \end{array} \right.$$

primary and conjugate dislocations are mixed dislocations.

(2) *Non-parallel dislocations*

a) different slip planes: $(\bar{1}\bar{1}\bar{2})$ and $(\bar{1}\bar{1}\bar{2})$, no possible boundary;

b) identical slip plane: $(\bar{1}\bar{1}0)$

$$\Omega // \mathbf{v} // [\bar{1}\bar{1}0]$$

primary and conjugate dislocations are mixed dislocations parallel respectively to $[\bar{1}\bar{1}2]$ and $[\bar{1}\bar{1}\bar{2}]$.

This table clearly shows that, at all events, slip polygonisation produces a lattice rotation axis $[\bar{1}\bar{1}0]$ in the present case. If one excepts case (1a) because edge dislocations are not expected to play a great role, and cases (1b) and (2) because cross-slip transfers via the $(\bar{1}\bar{1}0)$ plane are unlikely (section 3.2), then we have just no possible slip polygonisation at all. Therefore, as in part I, $(\bar{1}\bar{1}0)$ cross-slip transfers are a prerequisite for slip polygonisation between non-edge, non-parallel, primary and conjugate dislocations. Furthermore the formation of a subgrain boundary with at least some twist component in it is only possible by such transfers on the $(\bar{1}\bar{1}0)$ plane. This explains

why we fail to observe any lattice twist in our topographs. This indicates also that slip polygonisation (i.e. screening out of long range stresses) is likely to be much easier between edge than between non-edge primary and conjugate dislocations. Indeed, that is what we observed : only edge type tilt sheets are formed.

4. Results and interpretation. — Higher temperature tests have been performed only on specimen A (90 p.p.m. C), since it is likely that such a carbon content should not have much effects on the plastic behaviour at these temperatures. At low temperatures, on the other hand, the two A and B samples of different carbon content (90 and 16 p.p.m.) have been compared. Note that, because the $(112) [\bar{1}\bar{1}\bar{1}]$ slip system does not favour twinning, there has been no need to pre-train our samples, even at lower temperatures (123 K).

The experimental determination of the actual slip plane is not a simple task in b.c.c. metals. Our sample geometry does not make it easy ; on the lamella edge, all possible primary slip plane have the same trace since it contains the slip direction $[\bar{1}\bar{1}\bar{1}]$; only on the lamella plane itself, could traces be distinguishable : $(\bar{1}\bar{1}2)$ trace is along the lamella width, $[1\bar{1}0]$, while $(0\bar{1}\bar{1})$ or $(10\bar{1})$ traces make a 45° angle around it. However, such traces are in general wavy in nature, particularly at large strains ; moreover coarse kink bands at higher temperatures make difficult the observation of fine slip markings. At lower temperatures, 200 K and 150 K, Berg-Barrett topographs of the lamella plane (Fig. 7 and 10) show as clearly as possible (by extinction contrast) that slip lines do follow $(\bar{1}\bar{1}2)$ planes in an average way, as expected. At higher temperatures, 250 K and 295 K, such evidences are no more possible, due to coarse kink bands ; therefore we have mainly assumed, there, the effective primary slip plane to be $(\bar{1}\bar{1}2)$, on the basis of the existing literature for samples of comparable orientation and purity (e.g. [6]), and of the generally accepted trend that deviations to (110) slip planes seem to occur more likely at lower than at higher temperatures.

The experiments clearly show that some change in the strengthening mechanism occurs between 200 and 225 K. Therefore we report our results first in the high temperature, then in the low temperature range ; finally the transition range is detailed.

4.1 HIGH TEMPERATURE RANGE (295 K to 225 K).

4.1.1 Plastic deformation. — The deformation behaviour is characterized by the following points :

(i) The existence of two work-hardening stages on curves $\tau(\gamma)$ (Fig. 2). At 295 K, the stage I-stage II transition occurs at about 0.16 shear strain, and the work-hardening rate goes up from 4.2 kg/mm^2 to 9 kg/mm^2 . At 250 K, it occurs at about 0.27 shear strain and the hardening rate varies from 3.5 kg/mm^2 to 9 kg/mm^2 .

The elastic limit, as defined by the stress at which the activation volume is levelled down to a rough

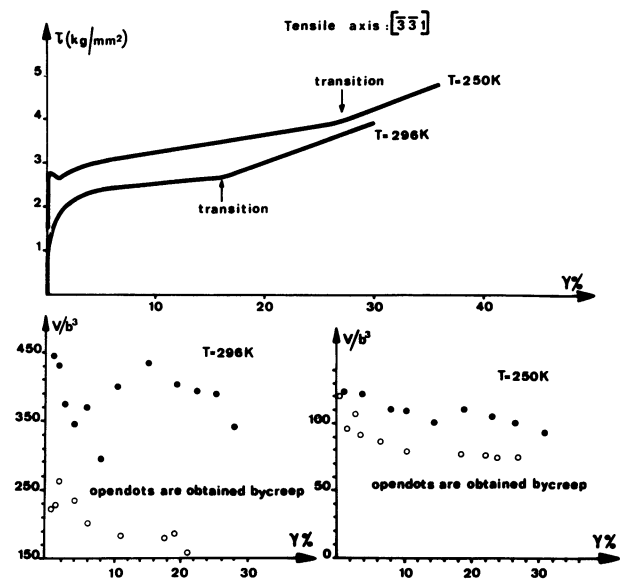


FIG. 2. — Sample A : High temperature range

$\dot{\gamma} = 2.5 \times 10^{-5} \text{ s}^{-1}$
Activation volume (v/b^3) versus resolved shear strain.

plateau (being of the order a few thousands b^3 in the pre-yield range), is 1.9 kg/mm^2 at 295 K and 2.8 kg/mm^2 at 250 K. These values compare well with similar values from literature [8], which confirms the relatively standard purity of our samples.

(ii) For both temperatures, activation volumes measured by stress changes during logarithmic creep are less spread out than those measured by stress relaxation ; this is consistent with results of part I. They decrease with increasing strain and become constant at about $180 b^3$ at 295 K and $75 b^3$ at 250 K.

(iii) Activation energies, as obtained by creep (temperature jumps), stay almost constant at about 0.8 eV, a behaviour similar to part I.

4.1.2 X-Ray observations. — The dislocation substructure has been examined by X-ray topography at 0.15, 0.20 and 0.30 strain (Fig. 3 to 5). Two kinds of tangles are revealed :

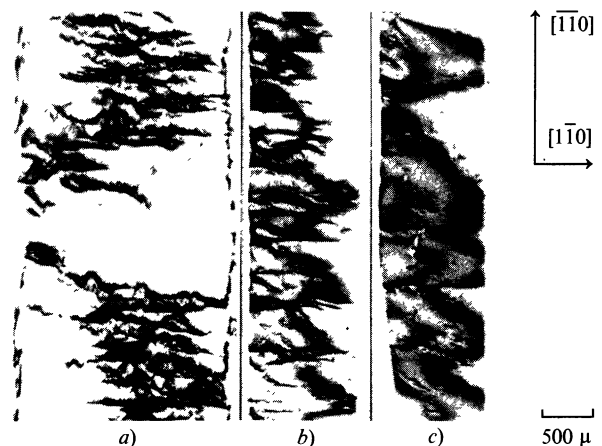


FIG. 3. — Sample A : $T = 296 \text{ K}$, (001) face, $g = [001]$

orientation axis : $[\bar{1}\bar{1}0]$
displacement axis : $[\bar{1}\bar{1}0]$

a) $\gamma = 30\%$; b) $\gamma = 20\%$; c) $\gamma = 15\%$.

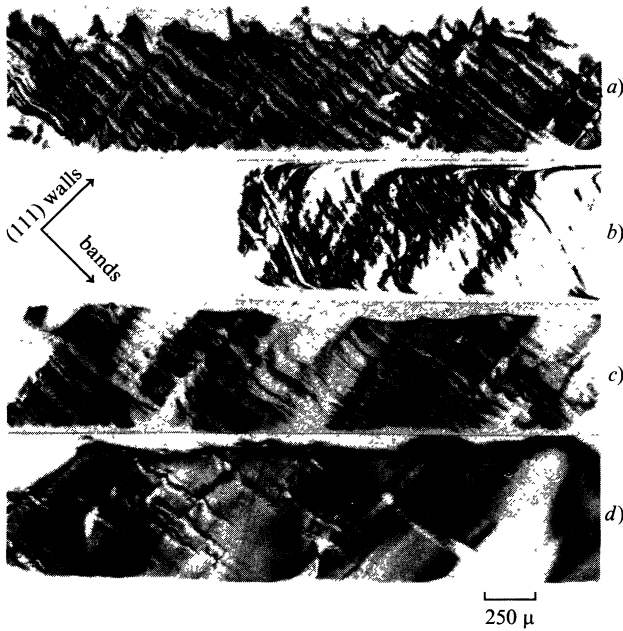


FIG. 4. — Sample A : $T = 296$ K, $(\bar{1}10)$ face, orientation axis : $[001]$, *a*) $\gamma = 30\%$, $\mathbf{g} = [\bar{1}00]$, displacement axis : $[010]$; *b*) $\gamma = 30\%$, $\mathbf{g} = [110]$, displacement axis : $[\bar{1}10]$; *c*) $\gamma = 20\%$, $\mathbf{g} = [010]$, displacement axis : $[\bar{1}00]$; *d*) $\gamma = 15\%$, $\mathbf{g} = [\bar{1}00]$, displacement axis : $[010]$.

(i) Rough dislocation walls parallel to $(\bar{1}11)$ planes, with alternate lattice tilts around the $[1\bar{1}0]$ primary edge direction, occur at 0.15 strain. Their spacing is rather large : at room temperature, it is of the order $600\ \mu\text{m}$ at 0.15 strain, $330\ \mu\text{m}$ at 0.20 and $170\ \mu\text{m}$ at 0.30; furthermore, it increases with decreasing temperature, and reaches $400\ \mu\text{m}$ at 0.30 strain and 250 K.

(ii) A much finer structure which strongly parallels the two work-hardening stages. During stage I, the substructure is quite homogeneous; only primary thin lines are slightly visible by extinction contrast. The onset of a series of heavy heterogeneous bands, stretched along the primary slip direction, is in contrast clearly connected to the stage I-stage II transition (Fig. 4). At room temperature, they appear at 0.15 strain then widen and multiply as stage II develops, till they cover the whole sample at 0.30 strain. Both primary and conjugate slip systems are apparent inside the band, while only primary lines are visible (by extinction contrast) outside. Detailed contrast analysis (Appendix A) shows the existence of dislocation sheets inside the band (Fig. 5), most of them extended roughly along the conjugate slip plane, with a rather small spacing ($20\ \mu\text{m}$). They induce lattice misorientations about an axis $\Omega = [1\bar{1}\bar{1}]$. Finally, from the cusp-shaped displacements they produce on primary lines when crossing them, it is likely that they contain numerous + and - dislocations.

4.1.3 *Interpretation.* — The observed dislocation substructure in stage I is typical of an easy glide mode. Except for the crude (111) tilt walls, presumably formed by the mutual capture of some primary edges, and much too widely spaced to harden the crystal, no other sheets, and no conjugate slip are detected, as expected (section 3.1). Consistently, stress-strain curves show only a slight hardening : there is probably no hindering of the primary screw dislocations by conjugate ones.

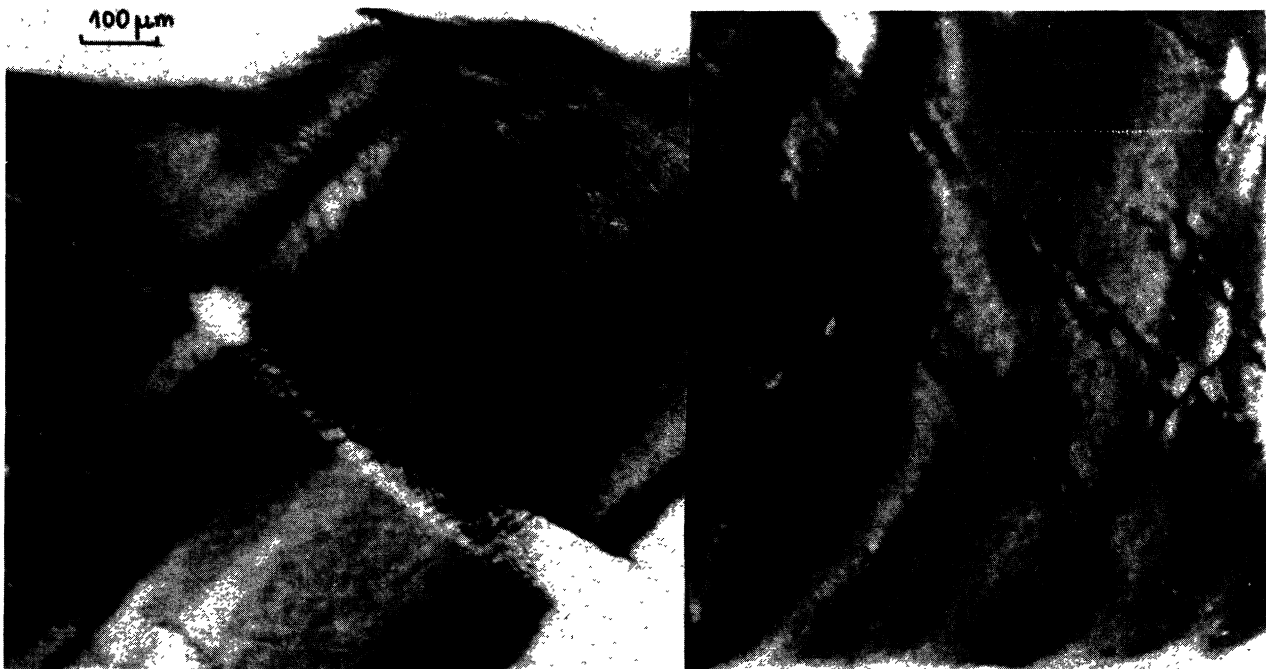


FIG. 5. — Sample A : $T = 296$ K : *a*) Detailed part from figure 4*d*; *b*) Vanishing of the displacement contrast observed in figure *a*) for $\mathbf{g} = [110]$.

In contrast, the appearance of a localized conjugate activity within bands at the stage I-stage II transition (Fig. 4d) demonstrates the crucial role of conjugate dislocations for developing stage II with a high work-hardening. It is reasonable to think that, in some regions along the primary slip lines, where internal stresses (built up during stage I by some tangling of primary screws) are made high enough to trigger locally conjugate slip against the lattice friction, some slip polygonisation starts to develop from attraction between the two slip systems. Doing so, part of the long range stress field is screened out but new short range obstacles are now created for further primary slip on the form of a localized conjugate forest. These are the sheets observed inside the bands on topographs (Fig. 4a, 5) and are at the origin of the sharp change in the work hardening rate. In turn, primary screws are held up against these hard points, generate internal stresses which trigger further polygonisation with conjugate screws, so the bands get wider and finally fill up the whole crystal (Fig. 4a).

X-ray topographs allow us to determine the nature of sheets inside the bands. Comparing the lattice rotation axis known from contrast analysis, $[\bar{1}\bar{1}]$, and what can be expected for slip polygonisation in table I, it is reasonable to take $l = 0$, i.e. $\Omega = [\bar{1}\bar{1}0]$. This is supported by a quasi-absence of orientation contrasts on $[001]$ topographs (Fig. 3). Finally, as stated above, the observed sheet plane is about the conjugate slip plane, i.e. $(\bar{1}\bar{1}\bar{2})$. This identifies the sheets as crude tilt boundaries, type (1a) in table I, and explains why no lattice twist is observed. In order to polygonise that way, not only conjugate screws have to be emitted from nearby sources but they have to be turned into the $(\bar{1}\bar{1}0)$ edge orientation in their own slip plane (without any cross-slip), as have also to be primary screws. In that sense lattice friction, the tendency of which is to stabilize the screw character, has to be overwhelmed by internal stresses generated by straining. This could explain why the strain for stage I-stage II transition has to be larger as the temperature goes down : at room temperature it is 0.15 while it is 0.27 at 250 K.

Of course, it is not claimed that this is the only conceivable picture of what occurs ; the presented observations are by no means thorough enough to support such a picture ; the preceding discussion is only given as a reasonable interpretation which fits consistently our experimental facts.

Probably similar dislocation sheets have been observed in Niobium also by Taylor *et al.* [18] using electron microscopy after comparable deformation conditions at room temperature (see their Fig. 7 in [18]). However both twist and tilt rotations are reported across the sheets, and the rotation axes do not seem to very clearly determined. It is possible that their general geometrical features are less easy to define at this much smaller scale.

4.2 LOW TEMPERATURE RANGE (BELOW 200 K). — In contrast with the preceding higher temperature range, the lattice friction is now so high that it prevails over any other hardening mechanism, and alone controls the whole plasticity, even in conditions of duplex slip at high strain. Because this behaviour is rather even, and is similar to what is reported in part I, we give below only a brief report of observations.

4.2.1 Plastic deformation (Fig. 6) :

(i) The elastic limit, about 5.5 kg/mm^2 at 200 K, increases very steeply and reaches 14 kg/mm^2 at 150 K and 15 kg/mm^2 at 123 K. Contrary to tensile tests at higher temperatures, which have been repeated on several samples, only one sample has been tested at 123 K, so that this value of 15 kg/mm^2 should be given with caution. At 150 K, the work-hardening rate is low. Figure 6 shows the stress-strain curve for sample B only ; the higher carbon content of sample A is only visible through a slight yield point, the lower stress of which agrees with preceding figures. At 123 K, the curve $\tau(\gamma)$ is flat and similar in shape up to necking.

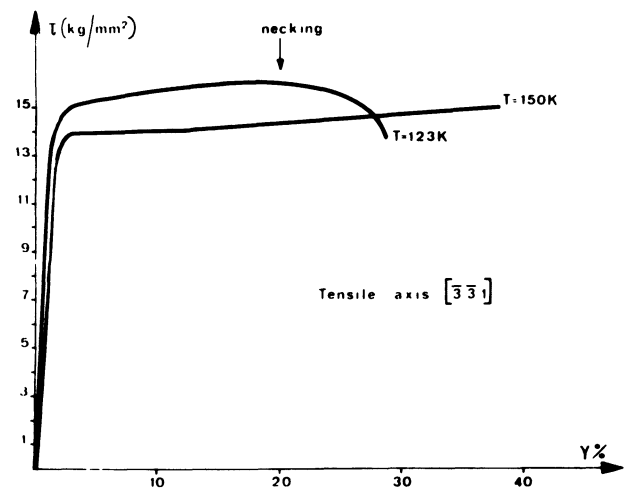


FIG. 6. — Sample B : Low-temperature range. Resolved shear stress-strain curve, $\dot{\gamma} = 2.5 \times 10^{-3} \text{ s}^{-1}$.

(ii) Creep activation energies have been measured at 150 K ; they are constant in strain at about 0.6 eV.

4.2.2 X-ray observations :

(i) The dislocation substructure is quite homogeneous up to strains as large as 0.3 (Fig. 7b, 8b). The preceding rough (111) walls have disappeared and only a weak, homogeneous, extinction contrast remains on the $(\bar{1}\bar{1}0)$ edge face of specimens, mostly along primary slip lines.

(ii) Beyond 0.3 strain, contrasted dislocation sheets extend throughout the crystal, along both the primary and the conjugate plane (Fig. 7a, 8a). These sheets are quite similar to the preceding ones, but they are now uniformly distributed. They give weaker contrasts, but still produce the same lattice rotations about

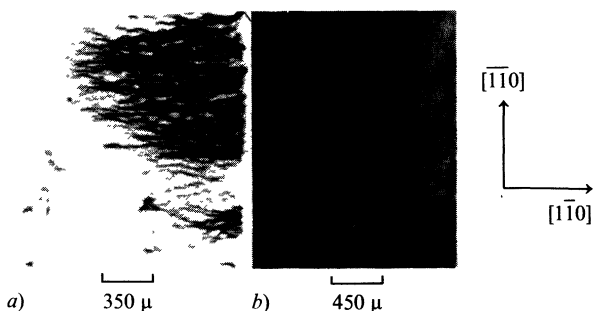


FIG. 7. — $T = 150$ K, sample B, (001) face, $g = [001]$
 { orientation axis : $[\bar{1}\bar{1}0]$
 displacement axis : $[1\bar{1}0]$
 a) $\gamma = 40\%$; b) $\gamma = 20\%$.

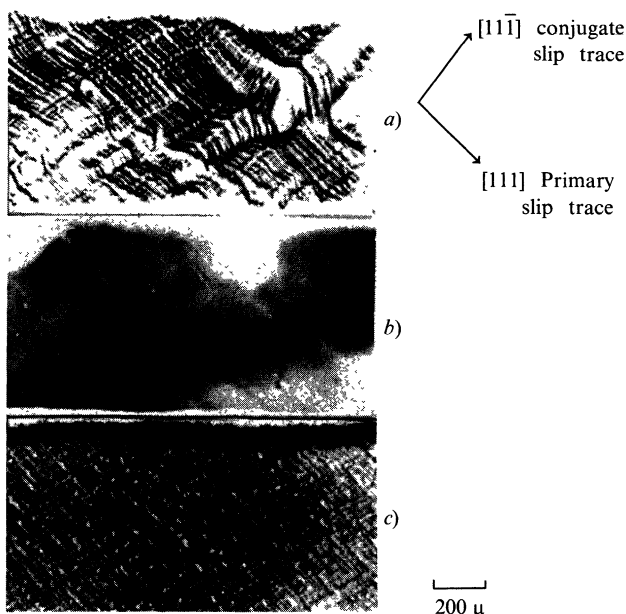


FIG. 8. — $T = 150$ K, $(\bar{1}\bar{1}0)$ face, $g = [100]$
 { orientation axis : $[001]$
 displacement axis : $[010]$
 a) $\gamma = 40\%$, Sample B; b) $\gamma = 20\%$, Sample B;
 c) Sample A, $\gamma = 40\%$.

$\Omega = [\bar{1}\bar{1}0]$. On the other hand, it can be noted they are closer spaced in the higher carbon sample A than in B (Fig. 8c), without apparent effect on the work-hardening rate.

4.2.3 Interpretation. — Measurements of activation volume below 200 K would have been clearly valuable to help in assessing a change in the hardening mechanism. Unfortunately, it has not been possible to perform them in the limited course of this study. Therefore our interpretation has to be only tentative in the light of experiment.

0.3 strain is the strain at which, due to stress axis rotation, the conjugate Schmid factor becomes as large as the primary one. Therefore, up to this strain, conjugate screws are not allowed to move under the only applied stress. Moreover the flow stress on primary plane is so high at these temperatures that

either primary screws should not tangle any more, or if they do, the produced internal stresses might not raise the total stress enough on conjugate planes, resulting in the absence of any conjugate activity together with an almost zero work-hardening rate (easy glide). The few conjugate slip lines sparsely observed in some regions on topographs (Fig. 8b) could be due to either some edge dislocations, or even some screws (due to some parasite stress), without noticeable effects on the general hardening. This is consistent with a very homogeneous dislocation substructure on topographs.

Beyond 0.3 strain on the other hand conjugate slip should be activated through the whole crystal (assuming no overshooting); because conjugate screws might now be reasonably mobile, interaction with primary ones should lead to a slight, uniform, slip polygonisation forming throughout the observed crude tilt walls $[1\bar{1}0]$ $(1\bar{1}2)$ or $(\bar{1}12)$ at high strain. But, due to their rather large spacing and again, to the high value of lattice friction, they are not expected to cause a noticeable work-hardening change.

This overall view of the plastic evolution with temperature and strain, makes it easier to discuss now a more surprising behaviour observed in transition range which occurs between 225 K and 200 K.

4.3 THE TRANSITION RANGE (225 K-200 K). — A somewhat unexpected work-hardening behaviour, with a harder stage I followed by a softer stage II, occurs on $\tau(\gamma)$ curves. Yet, the substructure is homogeneous in the stage I, almost without any lattice rotations, while dislocation sheets characterize the stage II. This phenomenon gradually develops with decreasing temperatures, is most clear at 200 K and disappears below.

4.3.1 Plastic deformation (Fig. 9) :

(i) At 225 K, the curve $\tau(\gamma)$ shows a kind of hump : the stage I is associated with a relatively high work-hardening rate (11 kg/mm^2) while the stage II has a lower hardening (5 kg/mm^2) from 0.22 strain and beyond. This hump occurs as well on sample A or B, with only the existence of a slight yield point for the former. At 200 K, the same hump is observed but at a larger strain (0.3). In sample A the work-hardening rate drops from 10 kg/mm^2 to 4 kg/mm^2 , while in sample B it is from 7 to only 1 kg/mm^2 .

(ii) At 225 K, activation volumes from stress relaxation tests are less scattered than at higher temperatures and become constant in strain much sooner ($50 b^3$). At 200 K, the same trend is clear.

(iii) Activation energy values from creep tests scatter between 0.5 eV and 0.7 eV, depending on strain.

4.3.2 X-Ray observations. — As has been said above, topographs are somewhat similar at 225 K or 200 K; only they are more typical at 200 K, so that it makes easier to describe them at this temperature.

(i) In stage I, up to strain 0.3 at 200 K, the disloca-

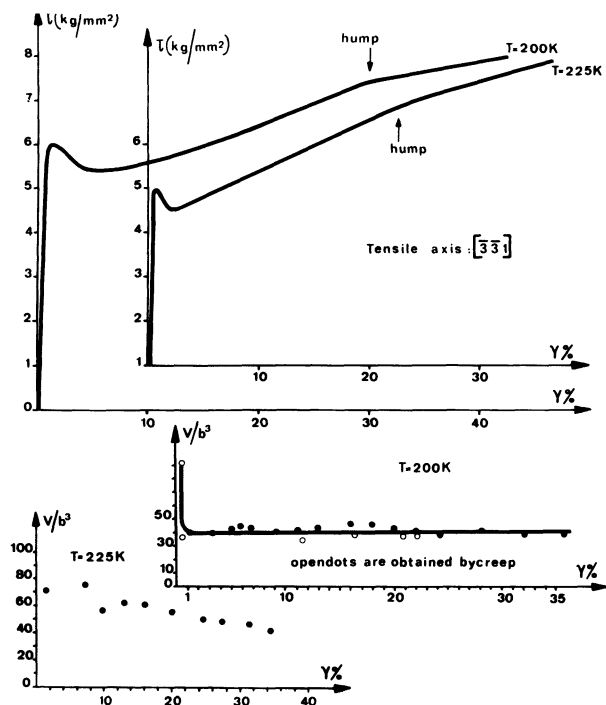


FIG. 9. — Sample A : Transition range
 { Resolved shear stress-strain curve, $\dot{\gamma} = 2.5 \times 10^{-5} \text{ s}^{-1}$
 Activation volumes (v/b^3) versus resolved shear strain.

tion substructure looks very homogeneous, with almost no slip traces at all (Fig. 11*b*).

(ii) As soon as the hump on $\tau(\gamma)$ curve is over, in stage II, mostly primary, but also more and more conjugate dislocation sheets appear (Fig. 11*a*). They still produce lattice rotations about $\Omega = [110]$ but, in contrast to the local bands obtained above 225 K, they are very uniformly distributed throughout the

crystal from the very beginning, as can be seen from topographs of the $(1\bar{1}0)$ edge face. For many aspects, they resemble the low temperature polygonisation substructure developed below 200 K at high strain (weak contrasts, rather large sheet spacings ranging from 50 to 75 μm).

These sheets are also visible on the lamella plane itself. Their traces follow roughly the common traces of both primary and conjugate planes (Fig. 10). At 225 K, some blurring occurs because then, the sheet-induced displacement contrast causes contrast lines to be simply translated as a whole (Appendix A). At lower temperatures, however, e.g. at 200 K, lattice rotations still decrease so that this translation is no longer visible, allowing the sheet structure to be observed more precisely (Fig. 10). It is seen that the traces are rather wavy about their average direction. Particularly interesting to note are some erratic zig-zags, inclined at about 45° around the average line. These could well be viewed as traces of local cross-slips on $(0\bar{1}1)$ and $(10\bar{1})$ planes.

Finally not much difference is observed between A and B samples at these temperatures.

4.3.3 Interpretation. — At first sight, the topographs do not show a substructure very different from what occurs at lower temperatures (although it could be argued that topographs of the lamella plane are a little more irregular). Yet a relatively high work-hardening rate is observed in the first stage, most surprisingly without any lattice rotations visible at the scale of Berg-Barrett topographs. These features have been confirmed to exist at 225 K and 200 K, on three different samples cut from either A or B crystals.

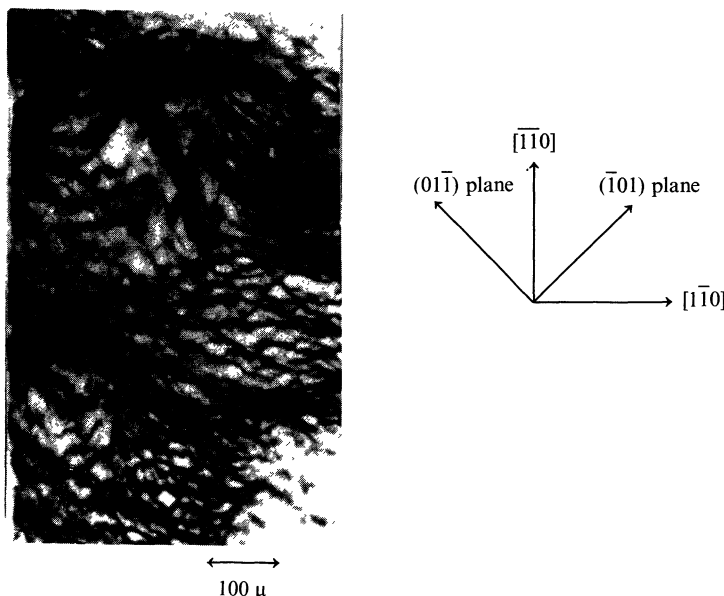


FIG. 10. — Sample A : $T = 200 \text{ K}$, (001) face, $g = [001]$
 { orientation axis : $[\bar{1}\bar{1}0]$
 displacement axis : $[110]$
 $\gamma = 40\%$.

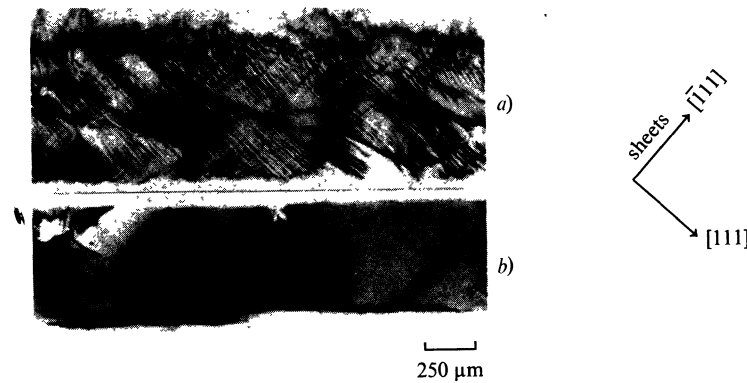


FIG. 11. — Sample A : $T = 200$ K, $(1\bar{1}0)$ face, $g = [100]$

$\left. \begin{array}{l} \text{orientation axis : } [001] \\ \text{displacement axis : } [010] \end{array} \right\}$
 a) $\gamma = 40\%$; b) $\gamma = 20\%$.

On the other hand, this behaviour is partly easier to understand when placed in the perspective of a balance between dislocation rearrangements generating strain hardening versus strain insensitive lattice friction, which favours the latter more and more as the temperature goes down. Thus, clearly, the crude slip polygonisation which develops in stage II looks similar to the corresponding crude sheet structure observed below 200 K, and has probably the same meaning. A conjugate activity is triggered through the whole crystal, as geometrical conditions for duplex slip are reached (critical strain for equal Schmid factor on conjugate and primary planes is 0.3). This activity generates in turn this loose polygonisation of edges into tilt walls $[1\bar{1}0]$ ($\bar{1}\bar{1}2$) or ($\bar{1}\bar{1}2$) described above. But its efficiency for relaxing the built-in internal stresses is very much dependent, apparently, on temperature. Below 200 K, being uniformly spread out, it gives almost no hardening at all; above 225 K, in contrast, it is very localized and induces a harder deformation stage; in between these two temperatures, while being uniformly distributed throughout the crystal, and relaxing a part of internal stresses accumulated during the stage I, a slight hardening still persists. To support this point we can recall the irregular and wavy nature of primary sheets on topographs, together with the stress favoured cross-slip on (101) and $(01\bar{1})$ planes (the Schmid factor of which ranges from 0.43 to 0.40 during deformation).

The first stage is still more puzzling. We observe there a relatively strong hardening under very homogeneous dislocation substructure conditions and constant activation volumes. Clearly, conjugate screws cannot polygonize at this stage. Instead, it is observed that primary screws harden the crystal contrary to their easy glide behaviour at comparable strains but higher temperatures. We have no explanations at the present for these experimental results; electron microscopy studies would be certainly valuable there, in order to clarify this transition range.

5. Conclusion. — This study corroborates the strong influence of lattice friction on strengthening mechanisms, dislocation rearrangements, and slip polygonisation at low temperatures, which was observed in part I. A transition range is again clear depending on the temperature, which occurs now between 225 K and 200 K.

Between room temperature and 225 K, although yielding is still controlled by lattice friction, stress strain curves show the usual two hardening stage scheme, an easy glide stage and a harder stage 2 which develops from bands within which local conjugate activity is clustered. Below 200 K, any rearrangement is inhibited by the high value of lattice friction, and the latter controls the whole plasticity. Curves $\tau(\gamma)$ are parabolic in shape, or even flat. In between 200 K and 225 K a region occurs where $\tau(\gamma)$ curves show a hump, being steeper in the first stage then becoming flatter at higher strains.

The crude slip polygonisation which develops for the present orientation is essentially the same in any case, being made of rough tilt walls, $[1\bar{1}0]$ ($\bar{1}\bar{1}2$) or ($\bar{1}\bar{1}2$), of mostly edge character and with apparently no visible twist component. Their building up does not need cross-slip, but rather glide of dislocations on their slip planes out of the screw orientation; so that they result from a balance between attractive dislocation rearrangements generating strain-hardening versus strain insensitive lattice friction, the latter being increasingly prevailing as the temperature decreases.

First stage is always a stage with a very homogeneous dislocation substructure (no lattice rotations if exception is made for the very crude (111) tilt walls observed at higher temperatures). Then the preceding walls, or dislocation sheets, appear (heterogeneous substructure) on the form of very localized bands at higher temperatures, which are associated with a sharp increase in work-hardening rate, or in strong contrast with a very loose, uniform distribution, being spread out through the whole sample, at tem-

peratures below 225 K, and they are then associated with a sharp lowering of work-hardening rate.

Finally, an analysis based simply on the possible perfect sub-boundaries without long range stresses which can be formed by primary and conjugate dislocation families, accounts reasonably well for the substructure formed in the course of deformation.

Acknowledgments. — The authors thank IRSID which supplied them with the as-grown α -iron single crystals and the « Ecole des Mines » of Saint-Etienne which measured the impurity content of our samples. They are very grateful to Dr J. Lecoq for his experimental help in deformation tests.

This work received financial support from D.G.R.S.T. contract n° 71-7-2785.

Appendix A : detailed study of the observed contrasts, particularly at 295 K and 250 K. — A.1 DETERMINATION OF THE MISORIENTATION AXIS Ω_{\perp} OF (111) WALLS :

- On the (001) face ($[\bar{1}\bar{1}0]$ axis vertical) the walls occur mainly by extinction contrast for the (001) reflection (Fig. 3) : therefore the misorientation axis $\Omega_{\perp} = |hkl|$ has no component in the $[\bar{1}\bar{1}0]$ direction, so we have : $h + k = 0$.

- Ω_{\perp} has a non-vanishing component on $[\bar{1}\bar{1}0]$: when the crystal is rotated by 90° the corresponding photograph shows an important orientation contrast.

- Ω_{\perp} has no component in the [001] direction ($l = 0$) : on the $(\bar{1}\bar{1}0)$ face, the walls appear by extinction contrast for the three reflections used (Fig. 4).

- On the other hand, on $(\bar{1}\bar{1}0)$ face, for the (010) and (100) reflections (Fig. 4a, c, d) the contrast lines are strongly displaced when they cross the walls ; besides, they appear to be straight for the $(\bar{1}\bar{1}0)$ reflection (Fig. 4b) : consequently, Ω_{\perp} has a non-vanishing component on the [100] direction ($h \neq 0$) and on the [010] direction ($k \neq 0$) ; but no component on the $[\bar{1}\bar{1}0]$ one ($h + k = 0$), as we have noticed above.

So, the whole set of our topographs shows that Ω_{\perp} is parallel to the $h[\bar{1}\bar{1}0]$ direction with $h \neq 0$. This is the direction of the primary edge dislocations.

Therefore (111) walls are one family *tilt* sub-boundaries. Furthermore the cusp-shaped contrast is evidence for the existence of numerous + and - dislocations inside the walls.

A.2 STUDY OF THE CONTRASTS OBSERVED IN THE BANDS. — On the outside of the bands, only primary slip lines are present. They are very fine and closed ; they occur by extinction contrast (Fig. 5).

Inside the bands both primary and conjugate slip systems are visible and contrasts are more prominent. Let $\Omega_s = [hkl]$ be the misorientation axis :

- On the $(\bar{1}\bar{1}0)$ face, for the (100) and (010) reflections (Fig. 5a), primary slip lines are displaced when they cross over the conjugate ones. This suggests the presence of dislocations sheets stretched on the conjugate planes ; this displacement contrast implies $h \neq 0$ and $k \neq 0$. Furthermore this displacement disappears for the $(\bar{1}\bar{1}0)$ reflections (Fig. 5b) :

$$h + k = 0 .$$

So, Ω_s is parallel to the $|h\bar{h}l|$ direction with $h \neq 0$. Besides, the occurrence of a cusp-shaped contrast shows that the sheets contain many + or - dislocations (Fig. 5a).

- On the other hand, on these topographs, there is no noticeable orientation contrast. This should suggest that $l = 0$, then $\Omega_s \parallel [\bar{1}\bar{1}0]$.

- At lower temperatures, the sheets spread on the whole crystal ; nevertheless they induce similar contrasts on the $(\bar{1}\bar{1}0)$ face.

Contrary to the high temperature case, the observation of the sheets is easier on the (001) face.

These ones are revealed mainly by extinction contrast, as it is expected for a misorientation around the $[\bar{1}\bar{1}0]$ direction (Fig. 7, 10). Such a misorientation should lead also to a displacement contrast.

As a matter of fact, primary and conjugate slip lines are identical on the (001) face. So, primary and conjugate lines are displaced *as a whole* : it is the cause of a blurred look of the topographs at high deformation.

References

- [1] COULON, G., LECOQ, J. and ESCAIG, B., *J. Physique* **35** (1974) 557.
- [2] LUFT, A., RICHTER, J., REITZENSTEIN, W. and FINKE, P., *Third Intern. Symp. Reinstoffe in Wissenschaft und Technik* (Akademie-Verlag, Berlin) 1972, p. 285.
- [3] LUFT, A. and KAUN, K., *Phys. Status Solidi* **37** (1970) 781.
- [4] KUBIN, L. P., Thèse d'Etat (Université de Paris Sud, Centre d'Orsay) 1971 p. 106.
- [5] BOWEN, D. K., CHRISTIAN, J. W. and TAYLOR, G., *Can. J. Phys.* **45** (1967) 903.
- [6] SPITZIG, W. A. and KEH, A. S., *Acta Metall.* **18** (1970) 611 and 1021.
- [7] STRÖHLE, D., SESTAK, B. and WILKENS, M., *Z. Metallkd.* **61** (1970) 642.
- [8] KEH, A. S., SPITZIG, W. A. and NAKADA, Y., *Phil. Mag.* **23** (1971) 829.
- [9] COULON, G., LECOQ, J. and ESCAIG, B., *Compte rendu de fin de contrat D.G.R.S.T. n° 71, 7, 2785, 1972, p. 29.*
- [10] LECOQ, J., Thèse de 3^e cycle. Université des Sciences et Techniques de Lille (1973).
- [11] JAUL, B., *Etude de la plasticité et application aux métaux.* (Dunod, Paris). 1965. p. 191.
- [12] GUIU, F. and PRATT, P. L., *Phys. Status Solidi* **6** (1964) 111.
- [13] NEWKIRK, J. B., *Trans. A.I.M.E.* **215** (1959) 483.
- [14] WILKENS, M., *Can. J. Phys.* **45** (1967) 567.
- [15] COULON, G., Thèse de 3^e cycle (Université des Sciences et Techniques de Lille). 1973.
- [16] AMELINCKX, S. and DEKEYSER, W., *Solid State Phys.* **8** (1959) 325.
- [17] LOUCHET, F., KUBIN, L. P., *Scr. Metall.* **9** (1975) 911.
- [18] TAYLOR, G., CHRISTIAN, J. W., *Phil. Mag.* **15** (1967) 893.